J Genet Resour2022;8(2): 218-235 *Homepage: http://sc.journals.umz.ac.ir/*

RESEARCH ARTICLE *DOI: 10.22080/jgr.2022.23855.1322*

J|G|R

Novel Cytological Findings on Gametophyte Development and Embryogenesis in Wheat (*Triticum aestivum* L.)

Kolsoum Azizi[1], Abdolkarim Chehregani Rad[1]* and Jalal Soltani[2]

[1] Department of Biology, Faculty of Science, Bu-Ali Sina University, Hamedan, Iran
[2] Department of Plant Protection, Faculty of Agriculture, Bu-Ali Sina University, Hamedan, Iran

ARTICLE INFO

Article history:
Received 10 June 2022
Accepted 12 August 2022
Available online 28 August 2022

Keywords:
Embryogenesis
Tapetum
Megasporogenesis
Microsporogenesis
Triticum aestivum L.

Corresponding authors:
✉ A. Chehregani Rad
chehregani@basu.ac.ir

p-ISSN 2423-4257
e-ISSN 2588-2589

ABSTRACT

A step-by-step study of the anther and ovule developments, sporogenesis, from pre-meiotic stages to anthesis in anthers and seed development in the ovary, was done in *Triticum aestivum* L. The results showed that the wall development at tetrasporangiate anthers was consistent with the monocotyledonous type. The anther locule was surrounded by two inner temporal cell layers, including the tapetal cells and the middle layer, and two outer permanent layers, including the endothecium and epidermis. Tapetum cells were observed as uni- or bi-nucleated in the maturity stage. Asynchronous cytokinesis during the meiosis of microsporocytes caused the formation of tetragonal tetrads. The mature pollen grains were monoporated and three-celled type. Different origins of the tapetum cells, the polarity of the tapetum cells, and callose formation around the microsporangial cells were novel findings. The ovule was bitegmic, tenuinucellate, and orthotropous initially, and anatropous in the late developmental stages. Chalazal megaspore was functional causing the formation of monosporic embryo sac type. Due to the proliferation of the antipodal cells, a modified Polygonum type of embryo sac was observed. The first zygote division occurred before the endosperm mother cell division and gave rise to equal cells. The nuclear endosperm was formed by dividing the nucleus of the endosperm mother cell. However, it became cellular in later stages. The endosperm involved three types of cells: an aleurone layer around the embryo sac, the endosperm cells around the embryo with dense cytoplasm, and the more giant and vacuolated endosperm cells away from the embryo. Deposition of the residual callose in the micropylar opening wall of the megaspores tetrad stage, variation in endosperm cell type, and some details of the developmental process are among the novel findings.

Please cite this paper as: Azizi K, Chehregani Rad A, Soltani J. 2022. Novel cytological findings on gametophyte development and embryogenesis in wheat (*Triticum aestivum* L.). *J Genet Resour* 8(2): 218-235. doi: 10.22080/jgr.2022.23855.1322.

Introduction

Poaceae (Gramineae) is the 15th most extensive family of flowering plants, with *ca*. 11,500 species and 768 genera (Soreng *et al.*, 2017). Poaceae crops play a crucial role in the food industry worldwide. The most economical speices in Poaceae, which is hexaploid wheator bread wheat *Triticum aestivum*, belongs to the tribe *Triticeae* and forms a subtribe *Triticinae* along with the genera *Aegilops, Taeniatherum, Secale, Connorochloa*, and *Hordeum* (Saarela et al., 2018). Wheat has a unique and strategic position in the human and animal diet for most of the world's populations. Due to its unique economic value, wheat biology has undergone extensive molecular, biochemical, morphological, and anatomical investigations. However, there are no detailed reports on its reproductive developmental stages (El-Ghazaly and Jensen, 1987). Due to the precise development schedule and the rapidness of

fertilization, wheat is introduced as an excellent plant for fertilization studies (You and Jensen, 1985). Cellular studies on sporogenesis, and male and female gametophyte development have estimated the duration of each stage (Bennett *et al.*, 1973). It is noted that by measuring some morphological characteristics of spikes, it is possible to identify the anthers developmental stages (Brown *et al.*, 2018). Various aspects of male sporogenesis and gametogenesis have also been studied (El-Ghazaly and Jensen, 1987). Despite such reports, gametogenesis in wheat has not been addressed in detail yet, and there has been little attention to the cellular behavior, cytological mechanism, the characteristics of sporophyte development, and correlation between sporophyte and gametophyte. Thus, we aimed at investigating micro- and mega-sporogenesis, micro- and mega-gametophytes development, fertilization, and seed development in wheat by a combination of fluorescence and light microscopy. The results were analyzed across a range of related taxa. This approach provides a better understanding of wheat reproduction processes for future genetic improvements and identification of the cellular mechanisms in fertilization. It may also help in elucidating wheat evolution and clarifying its interspecies phylogenetic relationships.

Materials and Methods

Wheat seeds (*Triticum aestivum* var. Mihan) were obtained from Hamedan Agricultural Research Center. The seeds were planted in the fall of 2018 at Bu-Ali Sina University, Hamedan Province, Iran, under green-house conditions with 60% humidity, at 20-25 ˚C and a normal photoperiod. After 2-3 months, inflorescences at various developmental stages (from the smallest to the largest) were collected. At least, 30 flowers were used for each stage.

The collected samples were fixed immediately in FAA_{70} [ethanol, acetic acid, and formaldehyde (17:1:2)] for 24-48 hours. The samples were dehydrated by 9 steps of increasing ethanol series (30%, 40%, 50%, 60%, 70%, 80%, 90%, and twice100% ethanol), 12 min in each step. Afterwards, they were transferred through 5 steps of ethanol-toluene series (3/4 ethanol+ 1/4 toluene, 1/2 ethanol +1/2 toluene, 1/4 ethanol + 3/4% toluene, and twice 100% toluene) for the elimination of ethanol and embedment of toluene. The specimens were then embedded in paraffin wax. The paraffin block content of buds was sliced with a thickness of 5-8 µm with a rotary microtome (Dideh Sabz Co, Iran). The serial sections were stained by hematoxylin-eosin by conventional methods (Chehregani *et al.*, 2009). Callose test was performed using aniline blue staining by conventional methods (Ramezani *et al.*, 2018). Slides were mounted on a microscope, and microscopic photographs were taken by different microscopy techniques, including a light microscope (LABOMED, LX50, Italy), a stereomicroscope (LABOMED, CZM6, Italy), and an epifluorescent microscope equipped with an ultraviolet light-emitting diode (Bell, Monza, Italy) as well as a camera, Bell Image Capture, model BLACKL. 3000, (3 Mpixel, Italy). Software (Qimaging Corporation, Austin, TX, USA) and power supply (PS-2 for mercury lamp, 100W/DC) were used for analysis. Both light and stereo microscopes were equipped with LABOMED digital camera, iVu 3100.

Results

Inflorescence and flower structures

Spike, which composed of spikelet units, is inflorescence of wheat. According to our observations (Fig. 1), the spikelets were situated in a zigzag form on the rachis axis (Fig. 1a). A number of florets on the zigzag-like axis of rachilla, formed a spikelet (Fig. 1b). Each floret was composed of five parts, *i.e.,* lemma, palea, lodicule, stamen, and pistil (Fig. 1c). Lemma and palea surrounded the reproductive part, and both contained awn. Lemma was larger than and located exterior to palea (Fig. 1c).

Flower development

According to the observations (Fig. 2), lemma and palea primordia were separated as the first organ of the floret meristem. Lemma and palea primordia were initially interconnected in their basal parts although their tops were free. They covered the generative meristem and reproductive organs until the fruit developed (Figs. 2a-c).

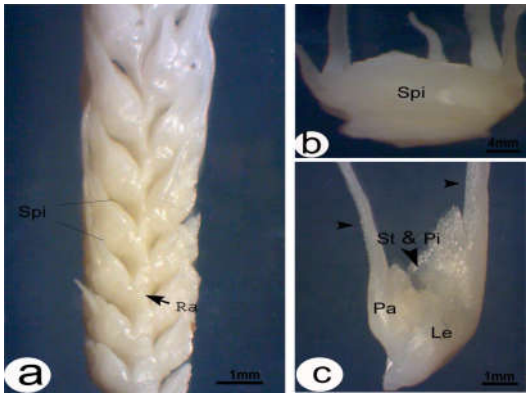

Fig. 1. Flower morphology of Triticum aestivum: **a**) A spike composed of spikelets (spi); **b**) Individual spikelet; **c**) Individual floret. Awn (arrowheads). pa: palea, pi: pistil, ra: rachis, st: stamen.

The lodicule primordium was the second organ to be separated from the meristem (Fig. 2a). With segregation and enlargement of lodicule primordium, the residual meristem moved upward and eventually differentiated from the stamen and the pistil (Figs. 2b, c). The florets had an axis with the ovary at the tip and a lemma at the base. The carpel was open at the early developmental stages (Figs. 2c, d) and then was closed (Fig. 2e). The sporangia and ovule went through the developmental stages simultaneously (Fig. 2f).

Microsporogenesis and male gametophyte development

As seen in Figs. 3 and 4, the microscopy studies showed that the stamens had tetrasporangiate anthers. Each microsporangium was independent of the others, and there was no common wall between them (Fig. 3a). The earliest stamens were the columns with a rectangular part, cross-section, filled with the homogeneous mass of meristematic cells (Fig. 3b). The volume of the anther primordium was increased by periclinal and anticlinal divisions. Periclinal division was specially observed at the outermost layer of its tissue (Fig. 3c). Afterward, the outer cell layer was differentiated from the epidermis, and the central cells followed the pathway of connective tissue differentiation (Fig. 3d). At each of the four rectangular anther angles, a sub-epidermal archesporial cell was formed (Fig. 3e) and produced a mass of undifferentiated cells, with mitotic divisions, that caused the formation of the tetra-lobe anther (Fig. 3f). The middle blades then separated microsporangia and distinguished them from each other (Figs. 3f-i). As a result of the peripheral division of one of the archesporial cells, two daughter cells were created (Figs. 3g, h). The inner cell, located in the sporangium center (Figs. 3i, j, k), and under mitotic divisions led to the formation of the microsporocytes (Figs. 3l, m). The microsporocytes or Pollen Mother Cells (PMCs) were prominent cells with large and central nuclei and dense cytoplasm (Fig. 3l). The outer cell, i.e., sub-epidermal cell, undergone two periclinal mitotic divisions for the anther wall formation. As a result of the first division, the endothecium was differentiated from the outer parietal cell (Figs. 3i- l). As a result of the second division, from the exterior cell, middle layer, and the interior cell, tapetal layers were differentiated (Fig. 3m). Eventually, the four-layered anther wall (from the exterior: the epidermis, the endothecium, the middle, and the tapetal layers) was formed by mitotic divisions of the second generation of archesporial cells (Fig. 3m). However, the microsporangia wall, in the proximate part of the connective tissue, was composed of two layers (Fig. 3m). Sub-connective tissue archesporial cells, in the first mitotic division of sub-epidermal parietal cells, were not divided (Figs. 3j, k). However, simultaneous with the second mitotic division of the sub-epidermal parietal cells, they undergone the periclinal mitosis division, produced the tapetum cells toward the sporangium center and middle layer toward the connective tissue (Fig. 3m). At the end of the pre-meiosis stage, the tapetum cells contained one nucleus, and the microsporangia were circular in the cross-sections (Figs. 3m, 4a). The callose wall began to form in the junction of the PMCs. Initially, it created a stellar appearance by permeating between the cells and then surrounded the PMCs (Figs. 4b-d).

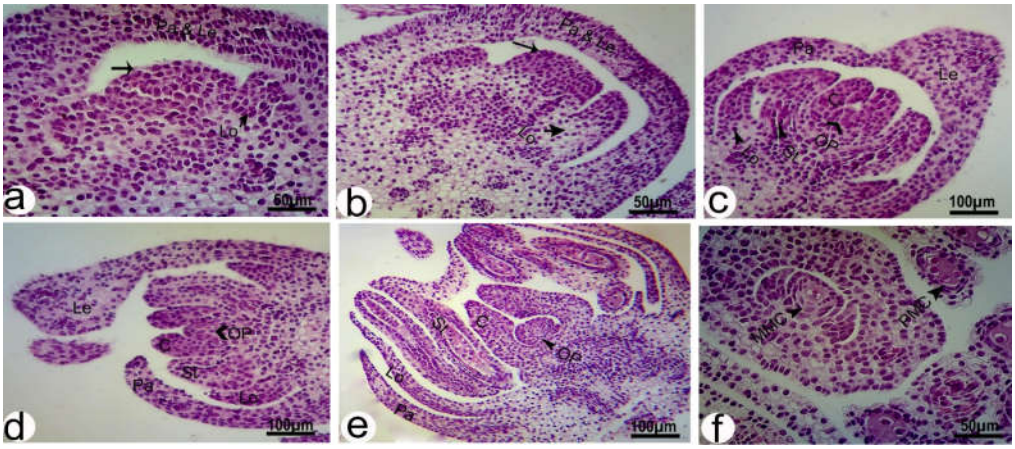

Fig. 2. Differentiation of wheat's floret meristem to the floret organs: **a**) The floret meristem. The Lodicule primordium (Lo) is differentiated from the floret meristem (arrow). The Lemma (Le) and the Palea (Pa) are interconnected, and covered all parts of the floret meristem; **b**) The growth of the lodicule primordium. Moves upward of the remaining meristem (arrow); **c**) Formation of all the primary organs of floret. The lemma and the palea are interconnected. The Carpel (C) is open; **d**) The floret primordium. The carpel is open. The lemma and the palea are separated; **e**) Individual floret. The carpel is closed; **f**) Synchronous development of the ovule and the anther. MMC: Megaspore Mother Cell, OP: Ovule Primordium, PMC: Pollen Mother Cell, St: Stamen.

The meiosis stages

Our microscopic observations, represented in Fig. 5, showed that with the onset of meiosis, the microsporangia expanded greatly in volume, became kidney-shaped in the transversal section, and the maturation of the tapetal cells occurred (Figs. 5a, b). At the early meiosis, the PMCs were composed of a united ring proximate to the tapetum layer, around a hollow center (Fig. 5a, b). Then, their chromatin was compacted, and cytoplasm density was reduced (Fig. 5a). Afterward, the chromatin fibers became tightly packed to form chromosomes at prophase I (Fig. 5c), and aligned at the metaphase plate at metaphase I (Fig. 5d). The paired chromosomes were segregated and pulled by spindle microtubules to the polar ends of the cell at anaphase I (Fig. 5e). Chromosomal fibers were uncoiled and became less dense, forming two daughter nuclei in telophase I (Fig. 5f). Golgi-derived secretory vesicles, following telophase I, were aligned in the cell plate, centrifugally (Fig. 5g). The fusion of those vesicles was expanded from the middle outwards until it reached the division site on the mother cell wall at cytokinesis I (Figs. 5h, i) and produced two cells. Still, the callose wall kept them together in a package and penetrated to the interwall of monomers dyad, the newly formed walls between the monads (Figs. 5j, k). Meiosis II commenced with prophase II (Fig. 5l), continued to metaphase II (Fig. 5m), anaphase II (Fig. 5n), telophase II (Fig. 5p), and cytokinesis II (Fig. 5q). Finally, tetragonal tetrads were formed with the asynchronous cytokinesis (Figs. 5t, u). The callose wall penetrated the newly intersporal wall, too (Figs. 5s, u). Deposition of the callose plug was observed in the distal part of the microspores in the tetrad stage (Fig. 5u). The first cell plate was perpendicular to the adjacent tapetum, i.e., along the distal-proximal axis of the microsporocytes (Figs. 5f, g, j, s). Meiotic asynchrony was observed in the sister cells belonging to a tetrad of microspores (Fig. 5o). The cubical tapetal cells had a dense cytoplasm with one nucleus at the beginning of the meiosis (Figs. 5a, c, d) and one or two nuclei during the meiosis (Figs. 5d, j, u). Tapetum's location at the microsporangia affected the tapetal cells staining. The color of the tapetum layer was pink at the adjacent of the connective tissue, whereas the tapetal cells seemed dark purple at the anther wall (Fig. 5a). Fluorescence microscopy confirmed the color differences, too. Indeed, the tapetum layer had a much intense auto-fluorescence at the adjacent connective tissue (Fig. 5b). The middle layer contained unstable, linear, and elongated cells with a limited number of cells (Figs. 5c, d, f, j) and disappeared at the end of the meiosis (Fig. 5u).

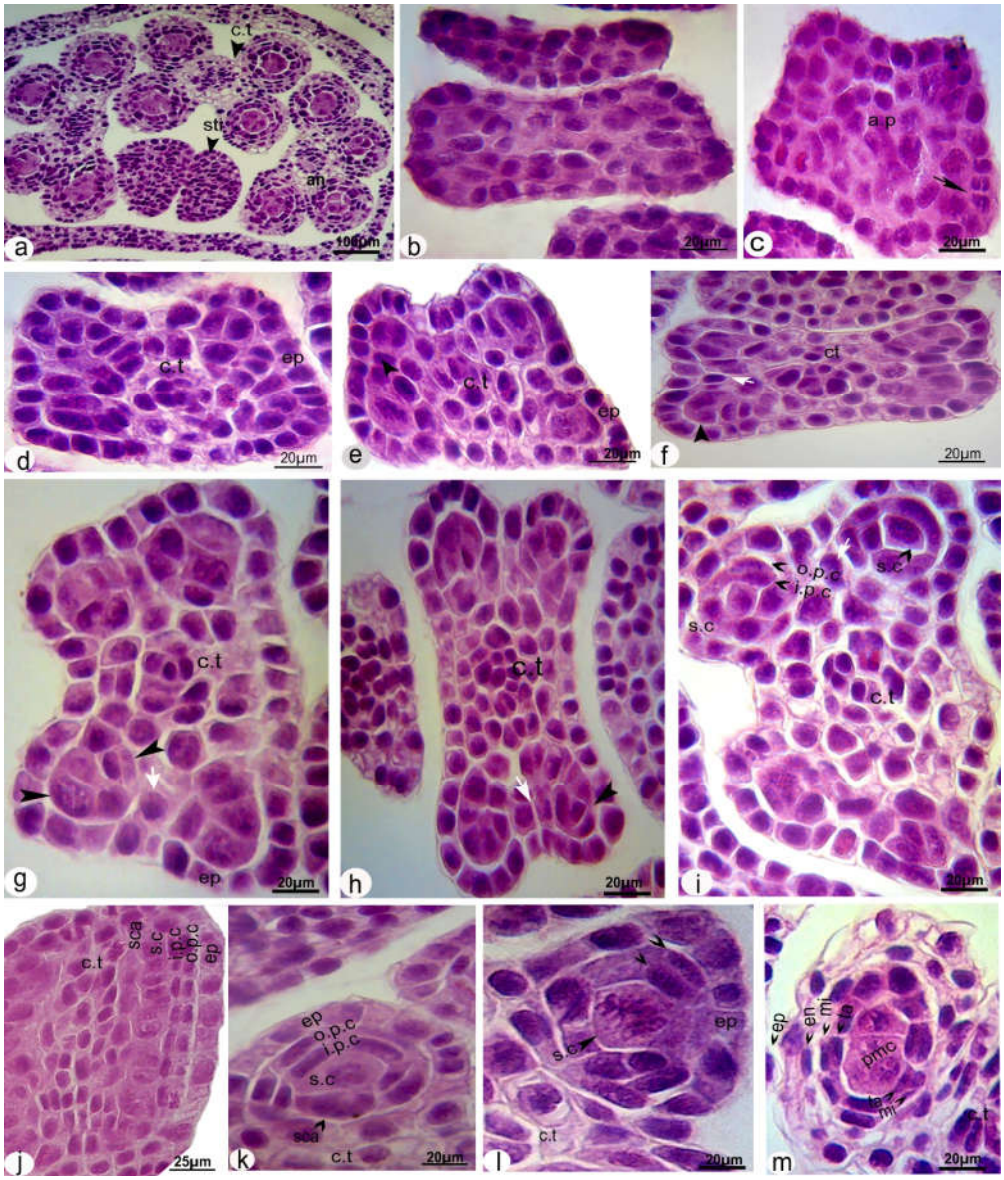

Fig. 3. Pre-meiosis in wheat's anther development: **a**) The stamens of the floret. Three tetrasporangiate anthers; **b**) The Anther Primordium (AP); **c**) Periclinal division at the outer most layer cell of anther primordia (arrow); **d** Differentiation of epidermis (Ep) and connective tissue; **e**) Differentiation of hypodermal archesporial cells. The beginning of mitosis division (arrow); **f**) The proliferation of archesporial cells by periclinal and anticlinal divisions. Formation of microsporangia (black arrowhead). The beginning of the differentiation of the middle blade (white arrow); **g**) Periclinal divisions of the sub- connective tissue arceosporial cells led to sporogenic cell formation at the center of locule (black arrowhead). Complete differentiation of connective tissue (white arrow); **h**) Periclinal divisions of the sub- epidermal arceosporial cells led to sporogenic cell formation at the center of locule (black arrowhead). Complete differentiation of connective tissue (white arrow); **i**) The division of parietal cell gives rise to Outer Parietal Cell (OPC) and Inner Parietal Cell (IPC). Outer parietal cell differentiates from the endothecium layer. The middle blade (white arrow); **j**) Longitudinal section of sporangia. The division of the sub-epidermal parietal cell gives rise to Outer Parietal Cell (OPC) and Outer Parietal Cell (IPC), but sub-connective tissue parietal cells are not divided; **k**) Transversal section of sporangia in developmental stage similar to the fig. j; **l**) Mitosis division of sporogenous cell to creates the Pollen Mother Cells (PMC). Parietal cell division (arrowheads); **m**) Complete the anther wall by the division of the inner parietal cell to the inner Tapetal Cell (Ta) and the outer middle layer. Differentiation of Pollen Mother Cells (PMC). Division of the sub-connective tissue parietal cells to inner tapetal cell and outer middle layer. An: Anther, CT*:* Connective Tissue, En: Endothecium, ML: Middle Layer Cell, Sty: style, SC: Sporogenous Cell, SCA: Sub-Connective Tissue Archesporial Cells.

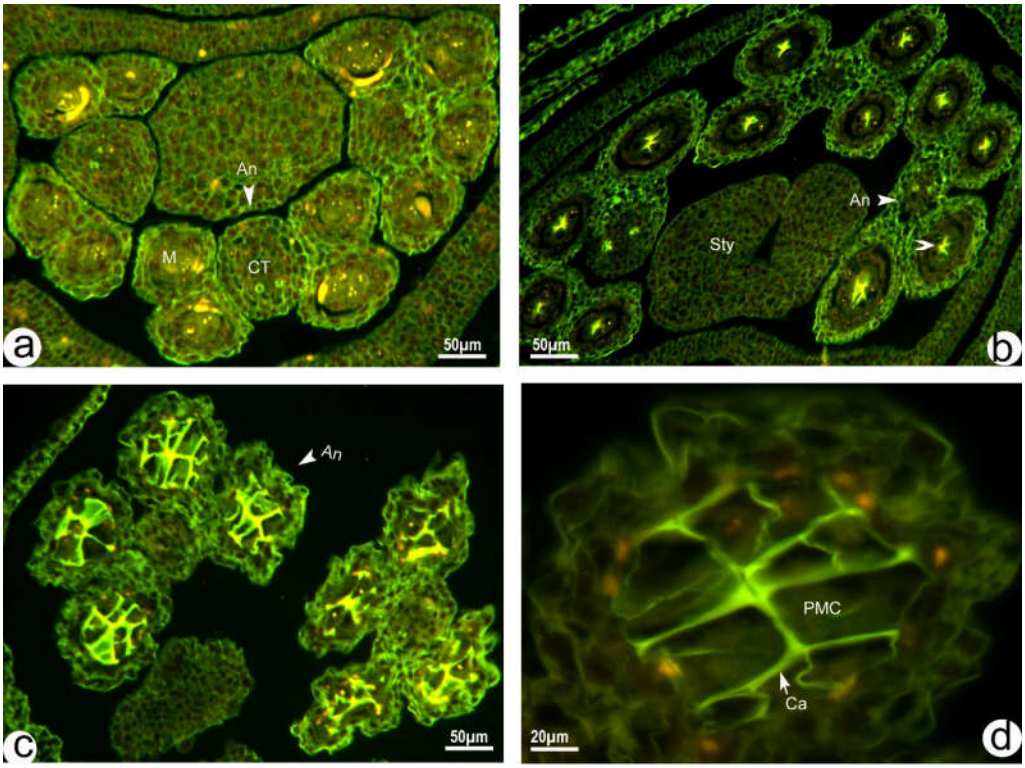

Fig. 4. Pre-meiosis stage in the anther development (fluorescence microscopy): **a**) Fluorescent microscope image of the Anther (An). It's not visible callose at microsporangia (M); **b**) Callose formation (white arrowhead) at the center of the microsporangial cavity (in the distal part of the pollen mother cells than the tapetum); **c**) The callosic wall completely surrounds the megasporocytes; **d**) The previous image with more zoom. Ca: Callose wall; CT: Connective Tissue, PMC: Pollen Mother Cells, *S*ty: Style.

Post-meiosis stages

As seen in Fig. 6, microspores produced in the previous stage (meiosis) were released by degeneration of the callose wall around the tetrad. Initially, microspores were not completely vacuolated, and their egg-shaped central nuclei (Fig. 6a) gradually moved to the margin by vacuolation of the cell (Figs. 6b, c). As the callose wall degraded, the secretary tapetum began to degenerate while preserving its location (Fig. 6b). Mitosis of the microspore resulted in the formation of the bi-nucleated pollen grain, consisting of a smaller generative nucleus and a larger vegetative nucleus (Fig. 6d). The generative nucleus which was undergoing mitosis (Fig. 6e) produced two spindle-shaped sperms (Fig. 6f). Therefore, the mature pollen grains were three-nucleated (Figs. 6f, g, h). Cytoplasm density around the generative nucleus was decreased, as it was divided to produce two sperms (Fig. 6e). The sperms were spindle-shaped in equatorial view (Figs. 6f, h). However, they were spherical-shaped in the polar view, with different sizes depending on the cutting site (Fig. 6g). The mature pollen grain was an irregular sphere (Fig. 6k). The single pore of the pollen grains was surrounded by an annulus (Fig. 6i) and had an operculum at its center (Fig. 6c). With the pollen maturation, the pollen tube germinated and moved toward the pore, and then passed the pore (Figs. 6j, k, l). At the onset, the pollen tube contents were non-dense (Fig. 6j). however, they became dense afterward (Fig. 6k) and passed the aperture (Fig. 6l). The anther dehiscence occurred with pollen grain maturity (Fig. 6m, n). The late anther wall was composed of the endothecium and epidermis layers. The endothecium cells reached their largest size and their lignocellulose fibers to the highest thickness (Fig. 6o). At the junction of the anther wall with the connective tissue, the endothecium fibers were thicker (Fig. 6p), and the anther wall pressure caused some of the connective tissues to burst (Fig. 6m). Thus, the anther was dehisced (Fig. 6n).

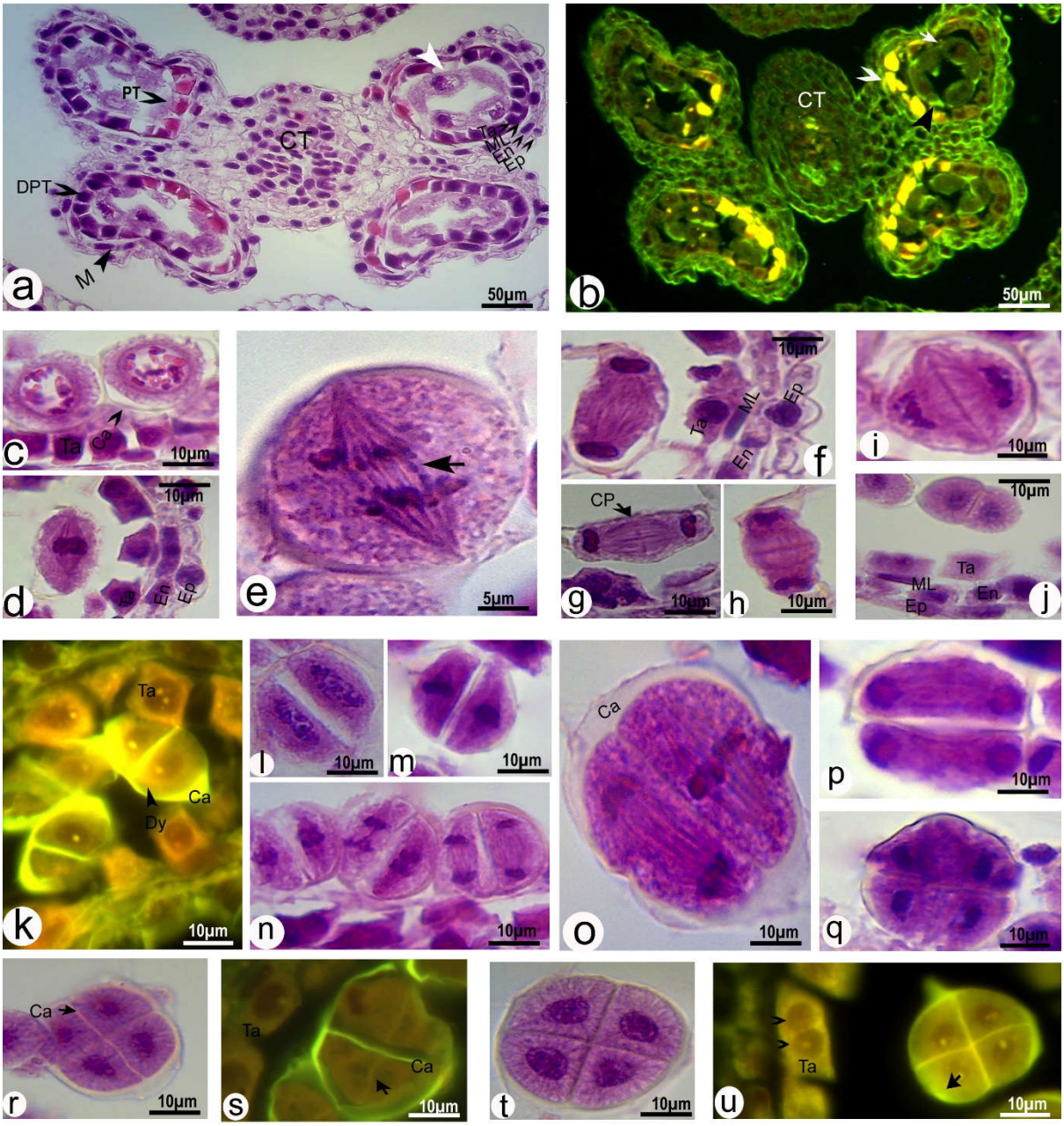

Fig. 5. The meiosis stages in the anther development: **a**) The tetrasporangiate anther. Tapetum layer close of connective tissue (PT) has a different staining. The ring of the pollen mother cells in close the tapetum (white arrowhead). The kidney-shape microsporangium (M); **b**) The intense auto-fluorescence of tapetum cells (white arrowhead) close the connective tissue confirms their different nature to other tapetum cells. The ring of pollen mother cells (white arrow); **c**) Prophase I; **d**) Metaphase I; **e**) Anaphase I. mitotic spindle (arrow); **f**) Telophase I; **g-i** cytokinesis. Centrifugal cell plate formation; **j**) Dyad; **k**) fluorescence microscopy of the callose penetration between the monads of microspores Dyad (Dy); **l**) Prophase II; **m**) Metaphase II; **n**) Different stages of anaphase II; **o**) Meiotic asynchrony in the sister cells belonging to a tetrad of microspores; **p**) Telophase II; **q**) Cytokinesis II; **r-t** Tetragonal tetrads; **r**) The end of the cytokinesis II; **s**) Fluorescence microscopy of formation of the callosic wall in cytokinesis II (arrow); **t**) Separation of tetrad monads completely; **u**) Fluorescence microscopy of the callosic wall envelop the outer and inner (intersporal) walls of the microspores. Bi-nucleated tapetum. The callosic plug in pore location (arrow). Ca: Callose Wall, CP: Cell Plate, CT: Connective Tissue, DPT: Dark Purple Tapi, Ep: Epidermis, En: Endothecium, ML: Middle Layer, PT: Pink Tapi, Ta: Tapi.

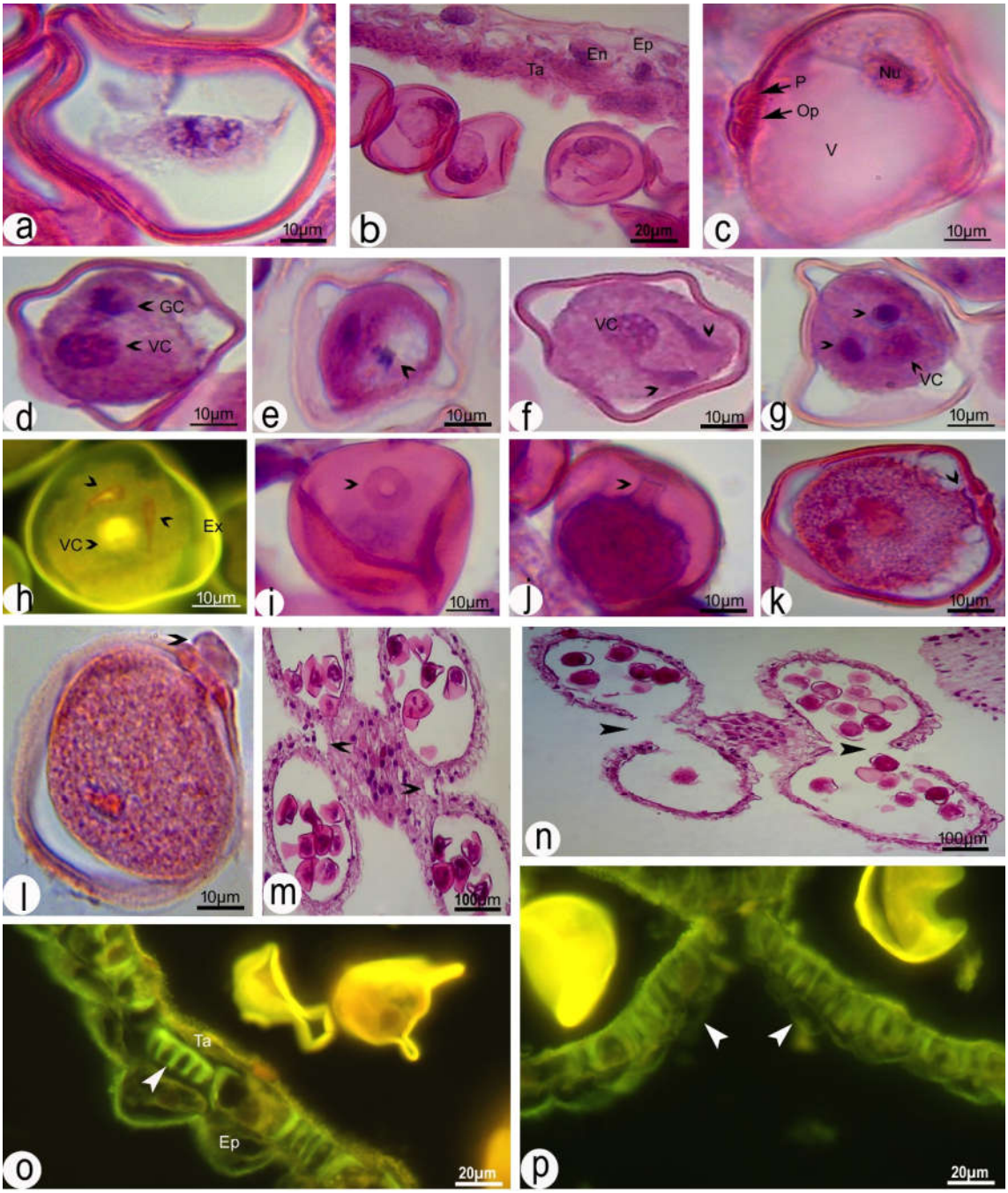

Fig. 6. The post-meiosis stage at the anther development: **a**) The free microspores stage. The soon after the callosic wall degeneration, nucleus have a central position; **b**) The vacuolated microspores with a peripheral nucleus. Tapetum (Ta) is degenerated gradually; **c**) The pore (P) of the microspore; **d**) Bi-nucleated pollen grain; **e**) Mitosis division of the generative nucleus (arrowhead); **f**) Three-nucleated pollen grain at the equatorial view. Sperms (arrowheads); **g**) Three-nucleated pollen grain at the polar view. Sperms (arrowheads); **h**) Auto-fluorescent property of the three-nucleated pollen grain; **i**) Pore (arrowhead); **j**) Germination of the pollen tube in the start of germination. Low density of the pollen tube content (arrowhead); **k**) The density of the pollen tube content is similar to that of the cytoplasm (arrowhead); **l**) The pollen tube exit from vegetative pore (arrowhead); **m**) Separation of some of the septum along the microsporangium wall (arrowheads); **n**) Anther dehiscence (arrowheads); **o**) Thickening of the fibers in endothecium that is shown with strong auto-fluorescent (arrowhead); **p**) The endothecium fibers are thicker at the dehiscence site of the anther (arrowheads). Ep: Epidermis, En: Endothecium, Ex: Exine, GC: Generative Cell, Nu: Nucleus, Op: Operculum, V: Vacuole, VC: Vegetative Cell.

Megasporogenesis stages

Microscopic images from pre-meiosis and meiosis (megasporogenesis) stages are represented in Fig 7. As shown, the ovary was superior and mono-carpel (Fig. 7a). The ovule was tenuinucellate, bitegmic, orthotropous at the beginning stage, with a very short funicule (Figs. 7b-d, 8a). The carpel was open when the ovular primordium was formed. The ovular primordium was a uniform cell mass enclosed by the ovary wall (Fig. 7a). At the early stages of the ovule development, a prominent subdermal cell was distinguished from the other cells at the tip of the ovular primordium, called the archesporial cell (Fig. 7b), and directly differentiated from the Megaspore Mother Cell (MMC) or the megasporocyte (Fig. 7c). The megasporocyte was a large cell with dense cytoplasm and a distinct nucleus (Figs. 7c, d). The megasporocyte, under meiosis I and II, firstly produced a dyad (Figs. 7e-g) and then a tetrad of the megaspores (Fig. 7h). The megaspores tetrad was linear and enveloped by the callose wall (Fig. 7i). Three of the megaspores were degenerated (Fig. 7j), while the chalazal megaspore was remained (Figs. 7j, k), acting as the functional megaspore (Figs. 7l, m). The functional megaspore became almost three-times larger than the others and formed the embryo sac mother cell (Fig. 7n). It had a dense cytoplasm with an intense auto-florescent property in its nucleus (Fig. 7o). In the megaspore tetrads, the callose wall of the chalazal megaspore was disappeared soon (Figs. 7j, k), but the callose walls of the other megaspores were gradually degraded (Fig. 7k). The residual of the megaspores callose walls was deposited on the micropyle opening (Fig. 7l, n). Since the callose emits an intense fluorescent light, fluorescent images confirmed its presence (Figs. 7m, o). The ovule was bitegmic (Figs. 7d-h). During the differentiation from the archesporial cell, the integuments were originated from the basal cells of the ovular primordium by periclinal division of the epidermal cells (Fig. 7b). The inner integument was developed before the outer integument, and both were bi-layers (Figs. 7c, d). The integument cells had only anticlinal divisions during the development. Hence, the number of the integument layers was persistent (Fig. 7i). The outer integument adhered to the inner integument during the development (Fig. 7i). The inner integument path was shorter, and the beginning point of the growth was higher than that of the outer integument, thus overtaking the outer integument (Figs. 7d, e-g). During the developmental stages of the embryo sac, the integuments were developing, and they were a get-together at the opposite end of the starting point (Fig. 7k, l). However, due to the rapid growth of the functional megaspore and the multiplication of its size, they diverged somewhat in the next stage (Fig. 7n).

Megagametogenesis stage

The results represented in Fig. 8 indicated that the functional megaspore had undergone three consecutive karyokineses to form an 8-nucleated embryo sac. The first round of division resulted in a 2-nucleate embryo sac whose nuclei were parallel to the longitudinal axis of the embryo sac (Fig. 8a). In the second round of mitosis, a 4-nucleated embryo sac was formed in which the nuclei were guided to each pole by a central vacuole. Similar to the prior stage, the nuclei had a linear arrangement in the 4-nucleated embryo sac (Fig. 8b, c). In the third round, an 8-nucleated sac was formed corresponding to the Polygonum type (Fig. 8d). As the embryo sac was developed, the nuclei began to differentiate, including a nucleus from each pole, called the polar nucleus, moved to the center of the embryo sac, and cytoplasm condensed around one of the micropylar nuclei (Fig. 8e). Also, as the integuments were approached in the mature embryo sac, a short micropyle canal was formed by the inner integument (Fig. 8f). However, the polar nuclei were joined (Fig. 8g) and migrated toward the micropylar pole (Fig. 8h). Subsequently, they were combined to produce a sizeable secondary nucleus. As the polar nuclei were located at the micropylar pole, a seven-celled embryonic sac was made by cellularization of the eight-nucleated embryo sac (Fig. 8h). The remaining three nuclei in the chalazal pole (Fig. 8g) were differentiated from the antipodal cells (Fig. 8h). Soon after the differentiation, they proliferated. Then, they form large and elongated polyploid cells (Figs. 8i, l). Following the development, the micropylar nucleus, which had a dense cytoplasm (Fig. 8e),

was differentiated from an egg cell with strong autofluorescence (Figs. 8g, j), and the remaining two nuclei in the micropylar pole (Fig. 8g) were differentiated from the synergids (Fig. 8h). However, the micropylar nuclei composed of two synergids, which were located toward the embryo sac center, and an egg cell which was at the micropylar opening at a more exterior location (near micropyle) than synergids, commonly called the egg apparatus (Figs. 8g, h). The synergids had a large vacuole toward the embryo sac center and a nucleus toward the micropylar end (Fig. 8h). During pollination, when the pollen tube entered the embryo sac, it passed from the cytoplasm of one of the synergids and destroyed it (Fig. 8k). When the sperm joined the polar nuclei, the polar nuclei had not been combined for the secondary nucleus yet (Fig. 8j). Two sperms fertilized the egg and the secondary nucleus. Then, the egg turned into the zygote (Fig. 8l), and the secondary cell became a triploid endosperm mother cell (Figs. 8k, l). The embedded callose walls in the micropyle pore persisted until the 4-nucleated embryo sac stage (Fig. 8c). however, they were degenerated in the 8-nucleus embryo sac (Fig. 8d).

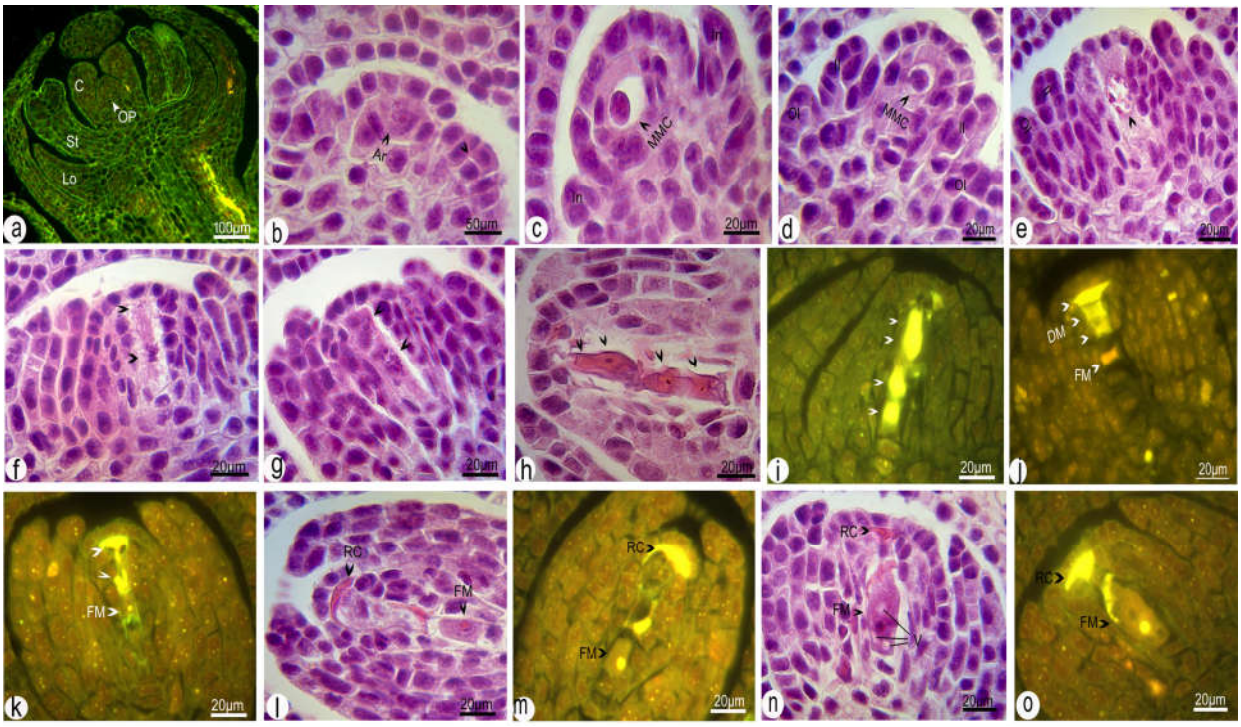

Fig. 7. Pre-meiosis and meiosis at the ovule development: **a**) Floret primordium (fluorescence microscopy); **b**) Hypodermal Archesporial Cell (Ar), periclinal division in epidermal cell and the beginning of Integument differentiation (In); **c**) The Megaspore Mother Cell (MMC); **d**) Germination both of the inner integument (II) and the outer integument (OI) before of the meiosis; **e-i**) Meiosis division; **e**) Prophase I; **f**) Anaphase I; **g**) Prophase II or dyad; **h**) Cytokinesis II or the tetrad of the megaspores; **i**) Auto-fluorescent property of the megaspores tetrad shows which they are enclosed in the callosic wall; j initiation of degeneration at the three micropylar megaspores (DM). Initiation of the callose disappearing in the chalazal Functional Megaspore (FM); **k**) Degeneration of the three micropylar megaspores (arrowheads). Differentiation of the chalazal Functional Megaspore (FM). The callosic wall is disappearing in the functional megaspore (green fluorescent); **l**) The Residual Callosic wall (RC) of the degenerated megaspores. Complete disappearance of the callosic wall of the functional megaspore; **m**) Strong auto-fluorescent property of the Residual Callose (RC) of the degeneration megaspores and functional megaspore's nucleus; **n**) The functional megaspore becomes very large. The remaining callose is visible in the micropylar end; **o**) image of the fluorescent microscope confirms the callose stability (arrowhead). C: carpel, OP: Ovule Primordium, St: Stamen, Lo: Lodicule.

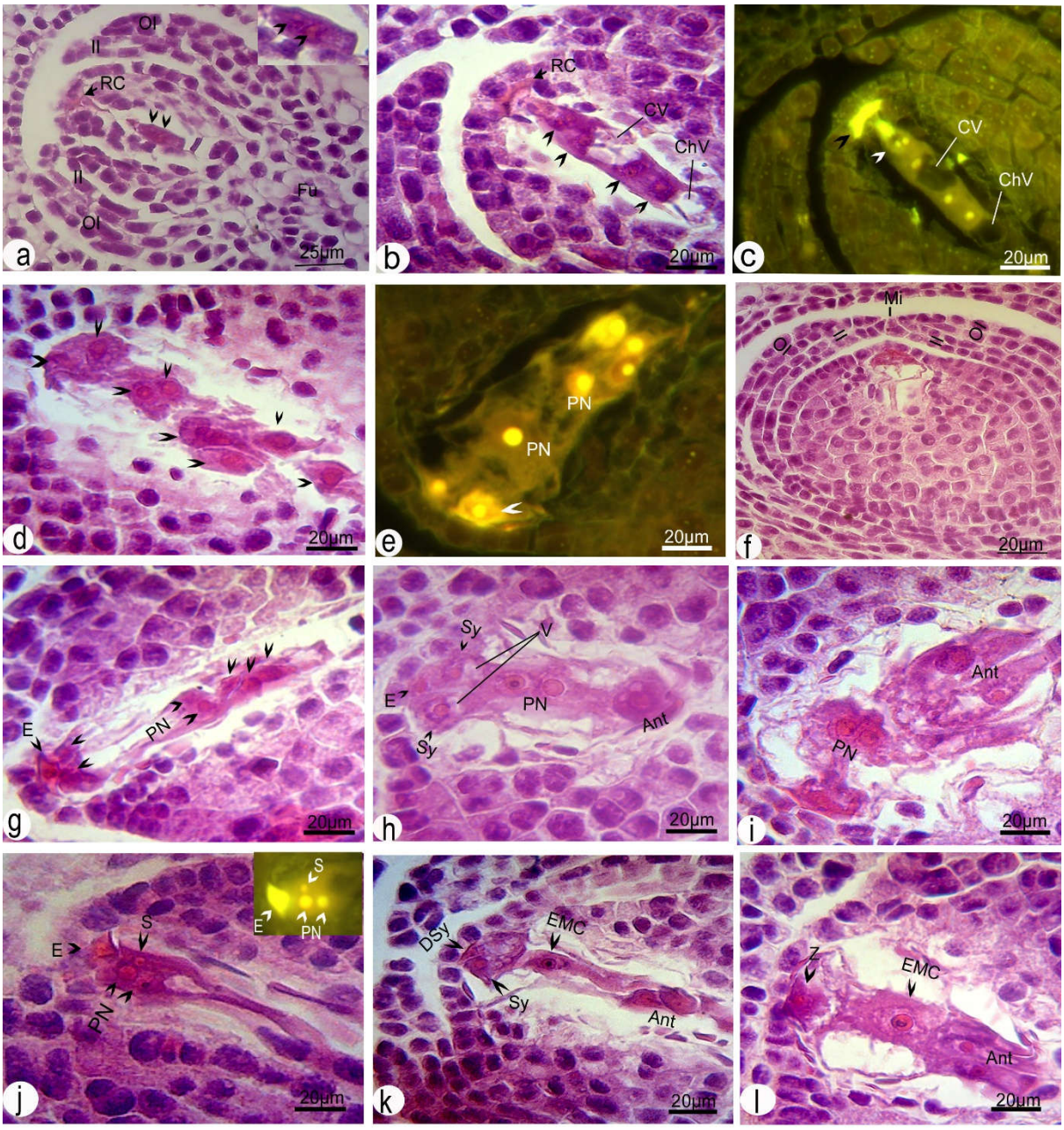

Fig. 8. Post-meiosis at the ovule development: **a**) Bi-nucleated embryo sac. Callose (white arrow); **b**) Tetra-nucleated embryo sac; **c**) Fluorescent image from the previous photo. Embryo sac nuclei have an intense auto-fluorescent. One of the nuclei has begun a new round of mitosis (white arrowhead). The callose remains up to this stage (black arrowhead); **d**) 8-nucleated embryo sac; **e**) A fluorescent image from the initiation of the differentiation at the embryo sac nuclei. The polar nuclei (PN) separate from the micropylar and chalazal ends, and move to the center of the embryo sac. start egg differentiation, a dense cytoplasm encloses the Egg Cell (E); **f**) Formation of Micropyle canal (Mi) in mature embryo sac by inner integument (II); **g**) Differentiation of the embryo sac nuclei. Near the chalazal end, the polar nuclei are joined together. The egg cell has a more outer position than the Synergid Cells (Sy); **h**) The polar nuclei are moving toward the micropylar end. Differentiated synergids have a large Vacuole (V) toward embryo sac center; **i**) Antipodal cells (Ant) become polyploidy; **j**) The Sperm (S) is placed near the polar nuclei. the polar nuclei have not yet been combined; **k**) As the pollen tube passes through one of the synergids, that cell is destroyed (DSy). Sperm and two polar nuclei give rise to Endosperm Mother Cell (EMC); **l**) Zygote (Z) is formed. Proliferation of the antipodal cells. ChV: Chalazal Vacuole, CV: Central Vacuole, Fu: Funicule, O: Outer Integument, RC: Residual Callose.

Embryogenesis and seed development stage

Our observation, as seen in Fig. 9 and Fig. 10, indicated that the embryogenesis began with egg fertilization. The first zygote division occurred before the endosperm mother cell division (Fig. 9a) giving rise to equal cells (Fig. 9b). The antipodal cells produced a spherical cell mass with intense auto-fluorescent property (Figs. 9b, c). When the endosperm mother cell began to proliferate, the antipodal cells started to degenerate (Fig. 9d). One of the synergids had remained after fertilization, then disappeared later (Figs. 9b, d). The nuclear endosperm was formed by dividing the nucleus of the endosperm mother cell (Figs. 9b-f). However, it became cellular in later stages (Figs. 9g-j). Initially, a spherical mass was formed (Fig. 9e), which was dispersed for the formation of one nuclear layer under the ovule shell (Fig. 9f) and then filled the entire ovule cavity by the proliferation of the nuclear endosperm (Figs. 9g-j). The endosperm involved three types of different cells, including a layer of aleurone (aleurone layer) around the embryo sac (Fig. 9k), the endosperm cells around the embryo with dense cytoplasm (Figs. 9g, j), and the more giant and vacuolated endosperm cells away from the embryo (Figs. 9h, j). During the development, the pro-embryo (Figs. 9a-d, i) produced a globular embryo (Figs. 9j, k) that later resembled a tennis rocket-shaped one (Fig. 9l). The single cotyledon of the embryo was formed in the later stages (Fig. 10a), and the embryonic axis was surrounded by the coleoptile (Fig. 10b). The endosperm around the embryo was consumed at this stage (Figs. 10a, b). The cross-section of the ovary during the seed growth indicated that the ovule was initially egg-shaped (Fig. 9a) while developing to a triangular-shaped one later (Figs. 9f-h). The chalazal-micropylar axis was rotated, creating the lateral position of the chalaza pole next to the micropyle, and the ovule became anatropous (Fig. 9e). During the seed development, the ovary and ovule shells unified (Figs. 9i, k), and as the ovary rotated, a groove was created on the seed. The ovary shell hairs were placed on the tip of the seed after fertilization and seed growth (Figs. 10c-e).

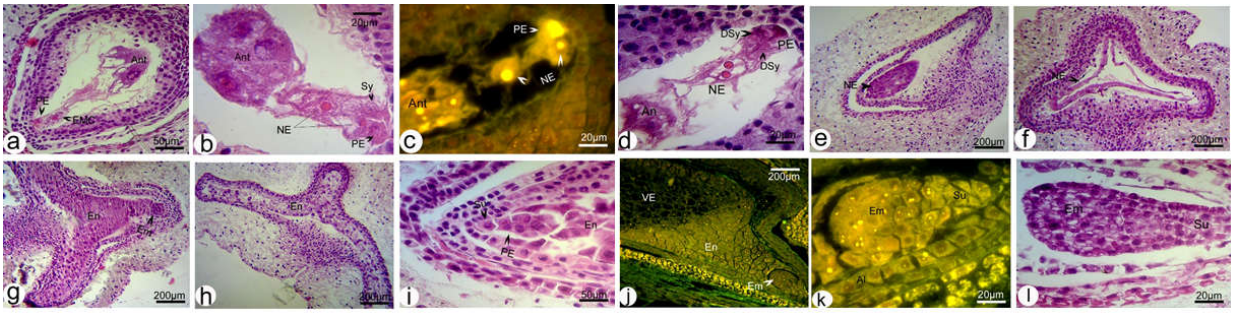

Fig. 9. Embryogenesis and the seed development: **a**) The zygote begins to proliferate before the endosperm mother cell and give rise to Proembryo (PE); **b**) A spherical mass produces during antipodal cells proliferation. Equal cells derived from the zygote division. The Degenerated Synergid (DSy); **c**) Auto-fluorescent image of embryo sac; **d**) As the endosperm mother cell divide, the antipodal cells begin to disappear; **e**) Transversal section of the seed (ovule). Rotation of the chalazal-micropylar axis. Initially, the nuclear endosperm is a spherical mass; **f**) The ovule enlargement and deformation at the transversal section. The nuclear endosperm is a layer below of the ovule shell; **g**)Transversal section from the lower part of ovule. The cellular endosperm cells with dense cytoplasm surround the embryo; **h**) Transversal section from the upper part of the ovule. The cellular endosperm cells are vacuolated and do not have dense cytoplasm; **i**) Longitudinal section of the ovule; **j**) Longitudinal section of the ovule. Endosperm cells with the dense cytoplasm surround the embryo (fluorescence microscopy); **k**) Joined ovule and ovary shell give rise seed shell (fluorescence microscopy); **l**) The embryo is resembling a tennis racket, with thickening suspensor; Al: Aleurone, Ant: Antipodal Cells, DSy: Degenerated Synergid, EMC: Endosperm Mother Cell, NE: Nuclear Endosperm, Su: Suspensor, VE: Vacuolated Endosperm.

Discussion

It was found that the stamens consisted of three tetra-sporangiate anthers attached to the filaments. Three-stamen plants, similar to wheat floret, as a characteristic representative of Poaceae, are considered as modern grasses (Clayton, 1990).

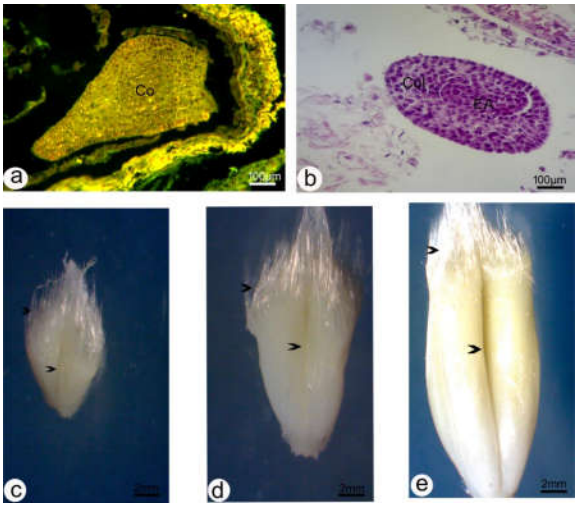

Fig. 10. Seed development: **a**) Cotyledon (Co) or scutellum (fluorescence microscopy); **b**) The Coleoptile (Col) surrounds the Embryonic Axis (EA). The endosperm surrounding the embryo is consumed by the embryo; **c-e**) The early, middle and late stages of the seed development. The seed has a groove and hairs at seed apex.

The middle layer of the anther, which was developed adjacent to the anther epidermis**,** was differentiated from the inner parietal cell during the mitosis division. This is consistent with the monocotyledonous type (Davis, 1966).

Furthermore, as seen, the tapetal cells were of the secretary one with one or two nuclei at the beginning of the meiosis that started to degenerate at the end of the meiosis. This is already reported by some other Poaceae members (Davis, 1966; Browne *et al.*, 2018). wang *et al*. (2003) also reported secretary tapetal cells in wheat. Uni or bi-nucleated tapetal cells have also been reported in some species of Poaceae alone (Schwab, 1971; Nakamura *et al.*, 2010).

A peculiarity observed in wheat was the polarity at the tapetum layer that caused a unique differentiation, i.e., in wheat, two types of cells were identified in the tapetum, some at the adjacent connective tissue (proximal tapetum), which were pink due to staining of their rich of protein cytoplasm with eosin, and the other tapetal cells at the anther wall (distal tapetum), which were dark purple due to staining of their cells, rich in nuclear material, with hematoxylin. The microscopic anther wall images showed that the distal and proximal tapetal cells had different origins. During the anther wall formation, the proximal tapetal cells differentiated from the archesporial cells positioned just under the connective tissue after the single mitosis they experienced. In contrast, the distal tapetal cells differentiated from the archesporial cells placed just under the epidermis after their second mitosis. It is reported in *Sorghum bicolor* that the anther wall, adjacent to the connective tissue, differentiates from the pre-existing connective cells (Christensen, 1972). However, considering the differentiated staining of the distal and proximal tapetal cells, we assume that the compounds accumulating in the proximal tapetal cells are different dramatically in nature from the distal tapetal cells. The fluorescence microscopy showed the inclusions by the intense auto-fluorescent property in the large vacuoles of the proximal tapetum. In the tapetal cells of *Arabidopsis*, auto-fluorescent vacuolar components involved the precursors of the pollen wall exine formation (Quilichini *et al.*, 2014). However, the auto-fluorescent property of the proximal tapetal cells was significantly higher in wheat than *Arabidopsis*. In contrast to *Arabidopsis*, wheat distal tapetal cells lacked auto-fluorescent property, indicating that there was a division of labor among the tapetal cells so that the proximal tapetal cells were mostly involved in the development of the pollen grains. In contrast, the distal tapetal cells were more important for nutrition.

The physical protection of the contents of anthers and regulation of the anther dehiscence were accomplished by the endothecium and the epidermis layers. In our study**,** as the anther developed, the endothecium layer grew significantly in thickness due to the continuous fibrous secondary thickening. This finding is in accordance with the former finding in Poaceae (Manning and Linder, 1990). The endothecium acted as a specialized dynamic system associated with microsporogenesis and pollen development. The results showed that in the early stages of the anther development, the endothecium primary cell wall allowed its stretching and further growth. However, the formation of the secondary cell wall in the endothecium cells in the late developmental stages of anther caused resistance against stretching and bending. Unlike endothecium, the epidermis layer became thinner

due to the cell dehydration, which created a motive force to anther opening. Dehydration of epidermis and secondary thickening of the endothecium played roles in the anther dehiscence (Nelson *et al.*, 2012). According to this, the anther opening resulted from the interaction between the endothecium layer and epidermis, depending on several parameters, e.g., natural characteristics of the epidermis and endothecium, hydration changes in the epidermis cells, and amount of secondary thickening in the endothecium cells. Dehydration of the epidermal cells reduced the length of the epidermis, causing tangential forces at the contact surface between the epidermis and endothecium, then transferring forces to endothecium, and unequal shrinkage of the bilayer as a result of endothecial resistance to bending due to endothecial secondary thickness, leading to the anther dehiscence (Nelson *et al.*, 2012).

Our findings showed that the secondary thickness of the endothecium layer was unequal along the anther wall. The anther walls at the junction of the connective tissue where dehiscence occurred, showed the most fibrous thickening, which increased the plasticity and tolerance to the extension in this site compared to the other parts of the endothecium layer (Nelson *et al.*, 2012). We propose that the location of thickenings along the endothecium layer is a key factor in determining the location of the anther opening. Since in anther walls, the secondary thickness was not formed, dehiscence did not occur (Wang *et al.*, 2015). We suppose that more resistance in the anther wall to bend the thicker parts resulted in the dehiscence of the anther wall in weaker sections adjacent to these parts and the release of the pollen grains.

Microsporogenesis and megasporogenesis started with the differentiation of microsporocytes and megasporocytes in the hypodermal cells. The individual archesporial cells, located at the center of the young anther locules, underwent the mitosis division, giving rise to the microsporocytes. Here, the microsporocytes were in direct contact with the tapetal cells and were enclosed by the callosic wall before entering the meiosis. During the microsporogenesis, the microsporocyte callosic wall surrounded the entire cell wall simultaneously (Ramezani *et al.*, 2018; Shirkhani *et al.*, 2019). One fundamental difference between the callosic wall in the megasporogenesis and microsporogenesis is polarity in callose formation surrounding the megaspore mother cell and megaspores tetrad (Ünal *et al.*, 2013). The thickness of the callosic wall is usually unequal around the megasporocyte and megaspores tetrad or begins to form and degrade at a specific point of the cell wall (Ekici and Dane, 2004; Musiał *et al.*, 2015). Since the callosic wall synthesis in wheat began in the contact point of the microsporocytes at the locule's center and then extended to the other parts of the microsporocyte wall, it indicated the polarity of the PMC in the microsporogenesis. Asymmetric depositions of callose at the beginning of the callose synthesis around the microsporosyte has already been reported in Graminaceous species (Christensen, 1972; Teng *et al.*, 2005).

As seen, the microsporogenesis along with meiosis I and Π, through the successive cytokinesis, resulted in the tetragonal tetrads enclosed by the callosic wall. The type of cytokinesis and the shape of the tetrad observed here correspond to what is described about wheat and Poaceae (Bennett *et al.*, 1973; Teng *et al.*, 2005). It seems that the orientation of the meiotic spindle is related to the callose polarity in wheat microsporocyte; meiosis I spindle is perpendicular to both the proximal-distal axis of the microsporocyte cell wall and the longitudinal axis of the microsporangia, while meiosis II spindle is parallel to the proximal-distal axis of the microsporocyte cell wall and perpendicular to the longitudinal axis of the microsporangia.

In the late microspores tetrad stage, the first signs of aperture and exine formation appeared (Wang and Dobritsa, 2018). After releasing the microspores from the tetrad, the monoporate pollen was developed. The pore consisted of an operculum and annulus. This particular shape of the aperture in wheat was a typical feature of Poaceae (Christensen, 1972; Nakamura *et al.*, 2010).

It is reported on wheat that the location of the pollen wall apertures is determined by the orientation of the spindle and cleavage planes in the meiosis division of the microsporocytes (Dover, 1972). Our observations on the relation between the polarity of the callose formation in

the microsporocytes and the spindle position of meiosis indicate that the aperture location on the pollen grain may depend on the situation of the microsporocyte geometry in the locule and the callose formation polarity.

The micrographs of the callosic wall surrounding the microspores tetrad indicated that additional callose deposits were revealed at the site for the future aperture formation. Similar data were reported on the several species belonging to different families (Albert *et al.*, 2011; Prieu *et al.*, 2017). The developmental relationship between the callosic plugs at the future apertural regions and the inhibition of the primexine deposition in aperture location are still unknown. Since the callose acts as a molecular filter (Heslop-Harrison, 1964), its possible mechanism can be explained as follows: increasing the callose thickness in future apertural regions may lead to a further decrease in the permeability of the primexine deposition or a slower enzymatic digestion of the callosic wall by callase. However, both of these lead to the passage of the primexin deposition phase. Thus, no exine deposition is formed, resulting in an aperture.

Pollen grains in wheat are three-celled, consisting of one large vegetative cell and two small sperm cells. Three-celled pollen grains are reported on wheat, rice, maize, *Hordeum vulgare* L., *Diarrhena*, etc. (Schwab, 1971; Bennett *et al.*, 1973; Itoh *et al.*, 2005; Zhou *et al.*, 2017). The pistil consists of a single carpel containing an ovule, a short style, and a two-lobed stigma. In the study, the ovules of wheat were tenuinucellate, bitegmic, and anatropous. The tenuinucellate and bitegmic ovules are typical for Poaceae (Greene, 1984; Lovisolo and Galati, 2007). The ovule of wheat was initially orthotropous, but as its development proceeded, the ovule rotation produced the anatropous ovule in the late developmental stage. This is in accordance with the former reports on *Diarrhena* and *Calamagrostis* spp. and wheat (Schwab, 1971; Greene, 1984). However, other types of ovule are found in Poaceae, e.g., Campylotropous (Mahalingappa, 1977), Hemianatropous (Greene, 1984), and Hemitropous (Lovisolo and Galati, 2007).

Here, in wheat, the megasporocyte was equivalent to the microsporocyte in the anther and underwent meiotic division producing the linear megaspores tetrad. This is in contrast with Bennett et al. (1973), who reported the T-shaped tetrad for wheat. However, similar to wheat, a linear tetrad is also observed in barley, rice (Cass *et al.*, 1985; Itoh *et al.*, 2005). However, both linear and T-shaped tetrads are commonly found in Poaceae (Leblanc *et al.*, 1995), although sometimes, only the T-shaped tetrad is found (Lovisolo and Galati, 2007). In accordance with Bennett *et al*. (1973), megaspores tetrads in our study were enveloped with the callosic wall. They had intense auto-fluorescence. Callose formation and disappearances did not begin simultaneously in all of the megaspores resulting in polarity as a factor for differentiation so that the starter megaspore gave rise to functional megaspore (Rodkiewicz, 1970), that is, chalazal megaspore in wheat, as reported in some Poaceae members (Greene, 1984; Lovisolo and Galati, 2007). The callosic wall around the three destroyed megaspores did not entirely disappear but deposited on the micropyle opening and closed until the 8-nucleated embryo sac was formed. It is reported for *Tripsacum* species that the fluorescent residues of degeneration megaspores remain for some time (Leblanc *et al.*, 1995). Since in the Poaceae family, the sporophyte tissues of the plant are responsible for directing the pollen tube close to the micropyle (Lausser *et al.*, 2009; Lausser and Dresselhaus, 2010), and since wheat micropyle was surrounded by two layers of cells, conduction of the pollen tube into the embryo sac was only done in the short path of micropyle thickness by diffusing the signals of synergids (Takeuchi and Higashiyama, 2012). Accordingly, one plausible interpretation is that deposition of the callosic wall in the micropylar opening can prevent the early entrance of the pollen tube into the embryo sac and also prevent the interactions of the female gametophyte-pollen tube. In other words, the callosic wall, as a barrier (Heslop-Harrison, 1964), inhibits the accidental entrance of the pollen tube to the embryo sac before the embryo sac maturation and synergids formation. The functional megaspore size is multiplied soon after differentiation. Consistent with our funding, giant functional megaspore is found in *Hordeum* (Cass *et al.*, 1985). The chalazal megaspore in wheat, like other Poaceae, forms a polygonum

type embryo sac that initially consists of two synergid cells, one egg, two polar nuclei, and three antipodal cells (Leblanc *et al.*, 1995; Lovisolo and Galati, 2007).

The mature synergids in wheat composed of two haploid cells with large vacuoles in the chalazal side and nucleus on the micropylar side, as observed in *Eleusine tristachya* (Lovisolo and Galati, 2007). They play a critical role in the attraction of the pollen tubes. One synergid for the signaling required the pollen tube attracting. However, the presence of two synergids increased the absorption signals (Higashiyama *et al.*, 2001). The results showed that the synergids were at the inner part of egg apparatus, near the central cell, and the egg cell was near the micropyle, contrary to the prior report on the location of egg and synergids in wheat (An and You, 2004). One of the reasons for the difference in the location of egg in Arabidopsis and wheat may be due to the different role of synergids, conduction of the pollen tube by sporophyte tissue in wheat (Lausser *et al.*, 2009; Lausser and Dresselhaus, 2010), and the pollen tube uptake in these two plants. One of the synergids in our study became degenerated before fertilization. Synergids are destroyed under cytoplasmic Programmed Cell Death (cPCD). They are first triggered in the cytoplasm and then reach the nucleus.

Based on the results, the vacuole was increased in size with increasing the size of the embryo sac. Our microscopic images showed several small vacuoles in the functional megaspore cell. One of the vacuoles became greater and produced a central vacuole in the 4-nucleated embryo sac. The central vacuole, as an organelle of the central cell, played an essential role in the megagametophyte development; with the survival of the megagametophyte cells and by maintaining the turgor pressure in the embryo sac cavity because of the thin cell wall or the absence of the cell wall in the embryo sac nuclei (Higashiyama *et al.*, 2001) in the first stage, and with the differentiation of the megagametophyte cells by polarization when pushing the nuclei toward the chalazal and micropylar poles (Ekici and Dane, 2004) in the second stage. In addition to the central vacuole, a smaller vacuole was located at the chalazal end of wheat embryo sac, being in accordance with the characteristics noted in some reports of Poaceae species (Wu *et al.*, 2011).

The antipodal cells are three haploid cells at the chalazal pole of the embryo sac, undergoing mitosis to become polyploid. Our results show that the antipodal cells became polyploid and proliferated and produced spherical cell mass. The number of the polyploid antipodal cells of wheat reaches about 30 cells (Bennett *et al.*, 1973). In wheat, as previously reported for the Poaceae family (Greene, 1984), because of proliferating at the antipodal cells, a modified Polygonum type is formed. However, in some species, for example, *Eleusine tristachya* (Lovisolo and Galati, 2007), the number of the antipodal cells is stable. The antipodal cells began to be destroyed, by nuclear-Programmed Cell Death (nPCD) (An and You, 2004), with the onset of the endosperm mother cell division. The two polar nuclei were combined with the other sperm to form a triploid endosperm mother cell, which was divided to develop an extensive endosperm tissue. The endosperm type of Poaceae is nuclear (Davis, 1966). Wheat endosperm is initially nuclear and then transforms into three types of cells. The results showed that the endosperm cells located at the peripheral of the embryo had dense cytoplasm. The cells far away from the embryo were vacuolated and had no electron-dense cytoplasm. An aleurone cell layer was visible that enclosed the two other parts of the endosperm, a storage cell layer for protein (Shewry and Halford, 2002).

So far, the details of the sporogenesis and gametophyte developmental stages were identified, and the possible mechanisms in the processes were described. The developmental stages indicate that *T. aestivum* can be a good monocotyledon model for the sporogenesis and gametophyte developmental studies. In particular, well-defined meiosis stages of microspores and polarity in callosic wall synthesis can be helpful in studies on meiosis and callose synthesis.

Author contribution statement

ACh and JS, as the supervisors, designed and conducted the study. KA, a PhD student, performed the field work and laboratory

analyses. All authors discussed the results and contributed to the writing of the manuscript.

Funding

This research did not receive any specific grant from funding agencies in the public, commercial, or non-profit sectors.

Acknowledgements

The authors would like to thank the research council of Bu-Ali Sina University, Hamedan, Iran.

Conflict of Interest

The authors declared no conflict of interest.

References

Albert B, Ressayre A, Nadot S. 2011. Correlation between pollen aperture pattern and callose deposition in late tetrad stage in three species producing atypical pollen grains. *Am J Bot* 98(2): 189-196.

An LH, You RL. 2004. Studies on nuclear degeneration during programmed cell death of synergid and antipodal cells in *Triticum aestivum Sex Plant Reprod* 17(4): 195-201.

Bennett MD, Rao MK, Smith JB, Bayliss MW. 1973. Cell development in the anther, the ovule, and the young seed of *Triticum aestivum* L. var. Chinese Spring. *Phil Trans Roy Soc B* 266(875): 39-81.

Browne RG, Iacuone S, Li SF, Dolferus R, Parish RW. 2018. Anther morphological development and stage determination in *Triticum aestivum*. *Front Plant Sci* 9: 228.

Cass DD, Peteya DJ, Robertson BL. 1985. Megagametophyte development in *Hordeum vulgare*. 1. Early megagametogenesis and the nature of cell wall formation. *Can J Bot* 63(12): 2164-2171.

Chehregani A, Malayeri B,Yousefi N. 2009. Developmental stages of ovule and megagametophyte in *Chenopodium botrys* L. (Chenopodiaceae). *Turk J Bot* 33(2): 75-81.

Christensen JE. 1972. Developmental aspects of microsporogenesis in *Sorghum bicolor*. Iowa State University.

Clayton WD. 1990. The spikelet. In: Chapman GP (ed). Reproductive Versatility in the Grasses. Cambridge, UK: Cambridge University Press 32-51.

Davis GL. 1966. Systematic Embryology of the Angiosperms. John Willey & Sons. Inc, USA.

Dover GA. 1972. The organization and polarity of pollen mother cells of *Triticum aestivum*. *J Cell Sci* 11(3): 699-711.

Drews GN, Koltunow A M. 2011. The female gametophyte. The Arabidopsis book/American Society of Plant Biologists 9.

Ekici N, Dane F. 2004. Polarity during sporogenesis and gametogenesis in plants. Biologia (Bratislava) 59: 687-696.

El-Ghazaly G, Jensen WA. 1987. Development of wheat (*Triticum aestivum*) pollen. II. Histochemical differentiation of wall and Ubisch bodies during development. *Am J Bot* 74(9): 1396-1418.

Greene CW. 1984. Sexual and apomictic reproduction in *Calamagrostis* (Gramineae) from eastern North America. American Journal of Botany 71(3): 285-293.

Heslop-Harrison J. 1964. Cell walls, cell membranes and protoplasmic connections during meiosis and pollen development. In Pollen Physiology and Fertilization *Edited by* Linskens HF. North-Holland, Amsterdam.

Higashiyama T, Yabe S, Sasaki N, Nishimura Y, Miyagishima SY, Kuroiwa H, Kuroiwa T. 2001. Pollen tube attraction by the synergid cell. *Science* 293(5534): 1480-1483.

Itoh JI, Nonomura KI, Ikeda K, Yamaki S, Inukai Y, Yamagishi H et al. 2005. Rice plant development: from zygote to spikelet. *Plant Cell Physiol* 46(1): 23-47.

Lausser A, Kliwer I, Srilunchang KO, Dresselhaus T. 2009. Sporophytic control of pollen tube growth and guidance in maize. *J Exp Bot* 61(3): 673-682.

Lausser A, Dresselhaus T. 2010. Sporophytic control of pollen tube growth and guidance in grasses. *Biochem Soc Trans* 38(2): 631-634.

Leblanc O, Peel MD, Carman JG, Savidan Y. 1995. Megasporogenesis and megagametogenesis in several *Tripsacum* species (Poaceae). *Am J Bot* 82(1): 57-63.

Lovisolo MR, Galati BG. 2007. Ultrastructure and development of the megagametophyte in *Eleusine tristachya* (Lam.) Lam. (Poaceae). *Flora* 202(4): 293-301.

Mahalingappa MS. 1977. Gametophytes of *Eleusine compressa* [millets, India]. *Phytomorph* 27: 231-239.

Manning JC, Linder HP. 1990. Cladistic analysis of patterns of endothecial thickenings in the Poales/Restionales. *Am J Bot* 77(2): 196-210.

Musiał K, Kościńska-Pająk M, Antolec R, Joachimiak AJ. 2015. Deposition of callose in young ovules of two *Taraxacum* species varying in the mode of reproduction. *Protoplasma* 252(1): 135-144.

Nakamura AT, Longhi-Wagner HM, Scatena VL. 2010. Anther and pollen development in some species of Poaceae (Poales). *Braz J Biol* 70(2): 351-360.

Nelson MR, Band LR, Dyson RJ, Lessinnes T, Wells DM, Yang C, …, Wilson ZA. 2012. A biomechanical model of anther opening reveals the roles of dehydration and secondary thickening. *New Phytol* 196(4): 1030-1037.

Prieu C, Toghranegar Z, Matamoro-Vidal A, Nadot S, Albert B. 2017. Additional callose deposits are located at the future apertural regions in sulcate, ulcerate, porate, colporate, colpate and syncolpate pollen grains. *Bot J Linn Soc* 183(2): 271-279.

Quilichini TD, Samuels AL, Douglas CJ. 2014. ABCG26-mediated polyketide trafficking and hydroxycinnamoyl spermidines contribute to pollen wall exine formation in *Arabidopsis*. *Plant Cell* 26(11): 4483-4498.

Ramezani H, Chehregani Rad A, Karamian R. 2018. Development of the male and female gametophyte in *Capsicum annuum* L. var. California Wonder. *Plant Biosyst* 152(6): 1-10.

Rodkiewicz B. 1970. Callose in cell walls during megasporogenesis in angiosperms. *Planta* 93(1): 39-47.

Saarela JM, Burke SV, Wysocki WP, Barrett MD, Clark LG, Craine JM, …, Duvall MR. 2018. A 250 plastome phylogeny of the grass family (Poaceae): topological support under different data partitions. *Peer J* 6: e4299.

Schwab CA. 1971. Floral structure and embryology of *Diarrhena* (Gramineae). Iowa State University.

Shewry PR, Halford NG. 2002. Cereal seed storage proteins: structures, properties and role in grain utilization. *J Exp Bot* 53(370): 947-958.

Shirkhani Z, Chehregani Rad A, Gholami M. 2019. Sporogenesis and gametophytes development in *Datura stramonium* L. (Solanaceae). *Braz J Bot* 42(1): 107-117.

Soreng RJ, Peterson PM, Romaschenko K, Davidse G, Teisher JK, Clark LG, …, Zuloaga FO. 2017. A worldwide phylogenetic classification of the Poaceae (Gramineae) II: An update and a comparison of two 2015 classifications. *J Syst Evol* 55(4): 259-290.

Takeuchi H, Higashiyama T. 2012. A species-specific cluster of defensin-like genes encodes diffusible pollen tube attractants in *Arabidopsis*. *PLoS Biol* 10(12): e1001449.

Teng N, Huang Z, Mu X, Jin B, Hu Y, Lin J. 2005. Microsporogenesis and pollen development in Leymus chinensis with emphasis on dynamic changes in callose deposition. *Flora* 200(3): 256-263.

Ünal M, Vardar F, Aytürk Ö. 2013. Callose in plant sexual reproduction. In Current progress in biological research. IntechOpen.

Wang, A, Xia Q, Xie W, Datla R, Selvaraj G. 2003. The classical Ubisch bodies carry a sporophytically produced structural protein (RAFTIN) that is essential for pollen development. *Proc Natl Acad Sci USA 100*(24): 14487-14492.

Wang H, Mao Y, Yang J, He Y. 2015. TCP24 modulates secondary cell wall thickening and anther endothecium development. *Front Plant Sci* 6: 436.

Wang R, Dobritsa AA. 2018. Exine and aperture patterns on the pollen surface: Their formation and roles in plant reproduction. *Annu plant rev online* 1(2): 589-628.

Wu CC, Diggle PK, Friedman WE. 2011. Female gametophyte development and double fertilization in *Balsas teosinte*, *Zea mays* subsp. parviglumis (Poaceae). *Sex Plant Reprod* 24(3): 219-229.

You R, Jensen WA. 1985. Ultrastructural observations of the mature megagametophyte and the fertilization in wheat (*Triticum aestivum*). *Can J Bot* 63(2): 163-178.

Zhou LZ, Juranić M, Dresselhaus T. 2017. Germline development and fertilization mechanisms in maize. *Mol Plant* 10(3): 389-401.